Transmission function of collinear acousto-optical interaction occurred by acoustic waves of finite amplitude

Alexandre S. Shcherbakov,[1,3] Adan Omar Arellanes,[1,4] and Sergey A. Nemov[2,5]

[1]*National Institute for Astrophysics, Optics & Electronics (INAOE), Puebla 72000, Mexico*
[2]*St. Petersburg State Polytechnic University, Polytechnicheskaya Str. 29, St-Petersburg 195251, Russia*
[3]*e-mail: alex@inaoep.mx*
[4]*e-mail: arellaneso@inaoep.mx*
[5]*e-mail: nemov_s@mail.ru*

Received April 9, 2013; revised July 26, 2013; accepted September 30, 2013;
posted October 15, 2013 (Doc. ID 188036); published November 12, 2013

New physical aspects of collinear acousto-optical interaction, occurred by acoustic waves of finite amplitude, are revealed and analyzed in crystalline materials exhibiting moderate linear acoustic losses. The analysis is performed in the regime of continuous traveling waves allowing a specific mechanism of the acousto-optic nonlinearity. Our consideration has shown that such nonlinearity together with linear acoustic losses is able to affect the transmission function inherent in collinear interaction. In particular, the mere presence of linear acoustic losses by themselves leads to broadening the width of the transmission function beginning already from very low levels of the applied acoustic power. Moreover, the transmission function exhibits a marked and quasi-periodical dependence on the applied acoustic power density, and that periodicity is governed by the linear acoustic losses. As a result, the transmission function can be significantly narrowed near isolated points at the cost of decreasing the interaction efficiency. These novelties related to collinear acousto-optical interaction accompanied by moderate linear acoustic losses have been studied and confirmed experimentally with an advanced acousto-optical cell based on calcium molybdate ($CaMoO_4$) single crystal and controlled by acoustic waves of finite amplitude.

OCIS codes: (190.2055) Dynamic gratings; (190.4410) Nonlinear optics, parametric processes; (230.1040) Acousto-optical devices.
http://dx.doi.org/10.1364/JOSAB.30.003174

1. INTRODUCTION

Collinear acousto-optical interaction by itself was initially revealed in the 1960s by Dixon [1], and starting from the 1970s it has been successfully studied and exploited in various applications, among which are tunable acousto-optical filters [2–8]. The conventional analysis of this phenomenon in terms of lossless plane waves was presented in a number of classical issues [9,10]. It allows the application of a given acoustic field approximation or, in other words, the regime of weak coupling, when the spatial distribution of an acoustic beam along a crystalline material is almost independent of the spatial distribution of light that leads to considerable theoretical and practical simplifications. In particular, 100% efficiency of light scattering may be achieved without any effect on the acoustic beam in this case, so the above-mentioned control can be repeated many times with almost no loss of acoustic energy. Moreover, an essential difference between velocities of light and ultrasound gives us an opportunity for applying the quasi-stationary approximation to the analysis of modern problems related to collinear interaction. In the past couple of decades, great progress has been made in acousto-optics, and now it is a widely used technique in the field of data processing [11,12]. Nevertheless, recently, the existence of a new branch in studies and applications of collinear acousto-optical interaction, which is associated with acousto-optical nonlinearity, for example, in the form of three-wave coupled states, has been manifested [13–15]. That is why we believe that it is a worthwhile investment to develop these investigations, because the objects under consideration here are closely connected with the above-mentioned nonlinearity in the regime of weak coupling. Within this consideration, we develop the exact and closed analytical model of collinear light scattering by continuous traveling acoustic waves of finite amplitude in a birefringent material with moderate linear acoustic losses. The most attention is paid to the distribution of the scattered light intensity, which can be considered as the transmission function of this process in the context of our analysis. In its turn, the width of the transmission function can be directly associated with the frequency resolution of the equivalent collinear acousto-optical filter. In so doing, we analyze the peculiarities of the effect conditioned by the acousto-optical nonlinearity, which leads to a measurable dependence of the transmission function on both the applied power density of acoustic waves of finite amplitude and the linear acoustic losses in crystalline material. Theoretically assumed novel properties of collinear acousto-optical interaction accompanied by nonlinearity and moderate linear acoustic losses are investigated experimentally with an advanced acousto-optical cell made of calcium molybdate ($CaMoO_4$) crystal and controlled by acoustic waves of finite amplitude.

2. THREE-WAVE COLLINEAR INTERACTION WITH PHASE MISMATCHES AND LINEAR ACOUSTIC LOSSES: CONDITIONS FOR EXTREMA OF LIGHT INTENSITY

Codirectional collinear acousto-optical interaction in a two-mode medium is governed by a triplet of combined partial differential equations [13] allowing the mismatch of wave numbers. The regime of weak coupling [14,15] is taken here, when two light modes are scattered by a relatively slow acoustic wave of finite amplitude, but light does not affect the acoustic mode. We approximate the velocities of light waves by the same value c, because practically the length of crystalline samples is less than 20 cm. Within the regime of weak coupling, the above-noted set of equations breaks down into an equation for the complex amplitude $U(x,t)$ of the acoustic wave and two combined equations for the complex amplitudes $C_0(x,t)$ and $C_1(x,t)$ of the transmitted and scattered light waves, respectively, passing along the x axes. At the initial step, we follow the analysis developed in Ref. [15] for the quasi-stationary continuous-wave regime for both the incident light and the acoustic wave $U = U_0 \exp(-\alpha x)\exp(i\varphi)$, where the amplitude U_0 and the phase φ of this wave are constant, while the factor α describes the linear acoustic losses. With the boundary conditions $C_0(x=0,t)=1$ and $C_1(x=0,t)=0$, one can find the stationary intensities of those light waves [15]:

$$|C_0(x)|^2 = \frac{\eta^2}{\sigma^2+\eta^2} + \frac{\sigma^2}{\sigma^2+\eta^2}\cos^2[G(x)-G(0)], \tag{1a}$$

$$|C_1(x)|^2 = \frac{q_0}{q_1}\frac{\sigma^2}{\sigma^2+\eta^2}\sin^2[G(x)-G(0)], \tag{1b}$$

$$G(x) = \frac{1}{\alpha}\left[-\sqrt{\eta^2+\sigma^2\exp(-2\alpha x)} + \eta\ln\left\{\frac{2\alpha}{\eta^2}\left[\eta\exp(\alpha x)+\sqrt{\sigma^2+\eta^2\exp(2\alpha x)}\right]\right\}\right]. \tag{2}$$

Here, $q_{0,1}$ are the constants of interaction for each light wave, and 2η is the mismatch of wave numbers inherent in the interacting waves (see physical details in Section 3). The parameter $q_0 q_1 U_0^2 = \sigma^2$ describes both the material properties and the acoustic power. When $\eta = 0$, one yields $G(x) = -\alpha^{-1}\sigma\exp(-\alpha x)$, so that Eq. (1b) takes the form [15]

$$|C_1(x)|^2 = \frac{q_0}{q_1}\sin^2\left\{\frac{\sigma}{\alpha}[1-\exp(-\alpha x)]\right\}. \tag{3}$$

Now, unlike Ref. [15] oriented to localizing the dissipative coupled states, the conditions of extrema efficiencies are applied to light scattering. Each extrema can be reached at $\eta = 0$, so that the positions of extrema are conditioned by the losses α and the parameter σ; see Eq. (3). The extrema in the scattered light distribution are given by

$$\text{Maxima: } G(x)-G(0) = \pi\left(N+\frac{1}{2}\right), \qquad N = 0,1,2,\ldots, \tag{4a}$$

$$\text{Zeros: } G(x)-G(0) = \pi M, \qquad M = 1,2,3,\ldots, \tag{4b}$$

where N and M are the numbers of maxima and zeros, respectively. These conditions lead to the equalities

$$\frac{\sigma}{\alpha}[1-\exp(-\alpha x)] = \pi\left(N+\frac{1}{2}\right), \tag{5a}$$

$$\frac{\sigma}{\alpha}[1-\exp(-\alpha x)] = \pi M. \tag{5b}$$

Because the left-hand sides of these formulas are limited, one can find that

$$N \le \frac{\sigma}{\alpha\pi}[1-\exp(-\alpha x)] - \frac{1}{2}, \tag{6a}$$

$$M \le \frac{\sigma}{\alpha\pi}[1-\exp(-\alpha x)]; \tag{6b}$$

i.e., the numbers N and M are restricted. Moreover, it is seen that $N \le (\sigma/\alpha\pi) - (1/2)$ and $M \le (\sigma/\alpha\pi)$ in the limit of $x \to \infty$.

First, let us consider the maxima. Equation (3) can be illustrated by the following 2D plot, which represents a few cross sections of the right-hand side of Eq. (5a) by planes $N = 0$, 1, 2; see Fig. 1. The unit-valued maxima of Eq. (3) under the condition imposed by Eq. (4a) are placed at the distances

$$X_N = -\alpha^{-1}\cdot\ln\left[1-\frac{\alpha\pi}{\sigma}\left(N+\frac{1}{2}\right)\right]. \tag{7}$$

For example, (1) when $\alpha = 0.1\ \text{cm}^{-1}$ and $\sigma = 0.5\ \text{cm}^{-1}$, one arrives at $N \le 1$ with $X_0 = 3.768$ cm and $X_1 = 28.55$ cm; (2) when $\alpha = 0.1\ \text{cm}^{-1}$ and $\sigma = 1\ \text{cm}^{-1}$, one yields $N \le 2$, wherein $X_0 = 1.709$ cm, $X_1 = 6.372$ cm, and $X_2 = 15.39$ cm (see Fig. 2); and (3) when $\alpha = 0.1\ \text{cm}^{-1}$ and $\sigma = 2\ \text{cm}^{-1}$, one has $N \le 5$ with $X_0 = 0.818$ cm, $X_1 = 2.687$ cm, $X_2 = 4.987$ cm, $X_3 = 7.980$ cm, $X_4 = 12.271$ cm, and $X_5 = 19.964$ cm. Together with this in the medium with much lower acoustical losses, let us say, for instance, with $\alpha = 0.01\ \text{cm}^{-1}$, one can find $N \le 15$ for $\sigma = 0.5\ \text{cm}^{-1}$ and $N \le 31$ for $\sigma = 1\ \text{cm}^{-1}$. Together with this, the graphical solution to Eq. (5a) gives another illustration for positions of the unit-valued maxima. For $N = 0$, these positions are depicted

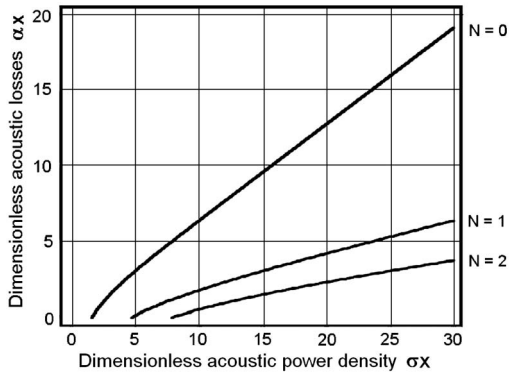

Fig. 1. 2D plot on the plane $(\alpha x, \sigma x)$ with lines corresponding to $N = 0$, 1, 2.

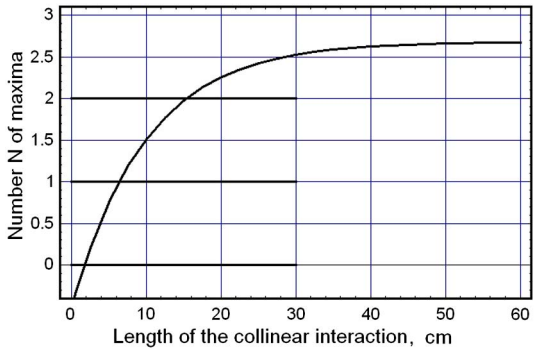

Fig. 2. Restricting the number N of unit-valued maxima; the particular case of $\alpha = 0.1$ cm^{-1}, $\sigma = 1$ cm^{-1}, and $N \le 2$ is shown.

by intersections of the curve $1 - \exp(-\alpha x)$ with horizontal lines $\alpha\pi/(2\sigma)$ in Fig. 3, where $\alpha = 0.1$ cm^{-1}.

At this step, one can analyze the zeros in the light intensity $|C_1|^2$ distribution. In so doing, Eq. (3) can be illustrated by a 2D plot, which represents a few cross sections of the right-hand side of Eq. (5b) by planes $M = 1, 2, 3, \ldots$, which is quite similar to Fig. 1. The zero-intensity points are placed at the distances

$$Z_M = -\alpha^{-1} \cdot \ln\left[1 - \frac{\alpha\pi}{\sigma} M\right]. \tag{8}$$

For example, (1) when $\alpha = 0.1$ cm^{-1} and $\sigma = 0.5$ cm^{-1}, one arrives at $0 < M \le 1$ with $Z_1 = 9.89$ cm; (2) when $\alpha = 0.1$ cm^{-1} and $\sigma = 1$ cm^{-1}, one yields $0 < M \le 3$, wherein $Z_1 = 3.77$ cm, $Z_2 = 9.89$ cm, and $Z_3 = 28.47$ cm (see Fig. 4);

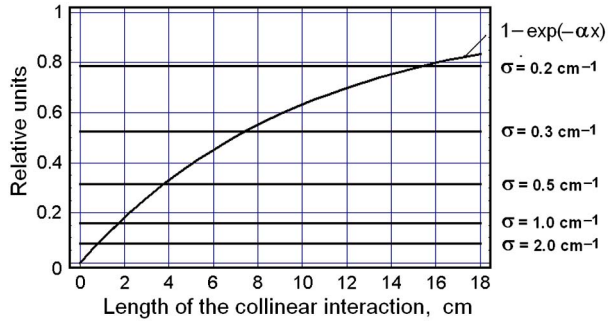

Fig. 3. Graphical solution to Eq. (5a); positions for the unit-valued maxima as a function of collinear interaction length. σ is a parameter for $N = 0$ and $\alpha = 0.1$ cm^{-1}.

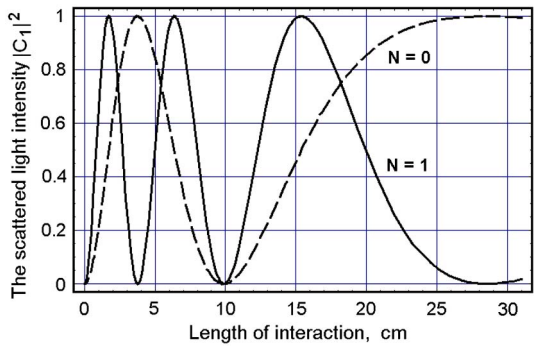

Fig. 4. Normalized scattered light distributions versus the dimensional length of interaction with $\alpha = 0.1$ cm^{-1}; the dashed line is for $\sigma = 0.5$ cm^{-1}, and the solid line is for $\sigma = 1$ cm^{-1}.

and (3) when $\alpha = 0.1$ cm^{-1} and $\sigma = 2$ cm^{-1}, one has $0 < M \le 6$ with $Z_1 = 1.708$ cm, $Z_2 = 3.77$ cm, $Z_3 = 6.386$ cm, $Z_4 = 9.89$ cm, $Z_5 = 15.37$ cm, and $Z_6 = 28.47$ cm.

Finally, Eq. (3) can be directly exploited for illustrating the light intensity dependences under consideration. In the above-noted approximation $q_0/q_1 \approx 1$ one can obtain the plots presented in Fig. 4. The extrema of each individual curve coincide with the calculated above values for X_N and Z_M; see Eqs. (7) and (8). At this step, one has to remind about the approximate character of the analysis developed in Ref. [15] and to note that Eq. (2) as well as Eqs. (7) and (8) are not valid for infinite distances.

3. TRANSMISSION FUNCTION FOR COLLINEAR ACOUSTO-OPTICAL INTERACTION WITH FINITE AMPLITUDE INPUT SIGNAL AND LINEAR ACOUSTIC LOSSES

It is well known [2–7] that the transmission function width (TFW) δf of collinear acousto-optical interaction is usually estimated by $\delta f = V/L$, where V is the acoustic wave velocity and L is the longitudinal aperture of crystal, i.e., the length of acousto-optical interaction. It is seen that this formula does not include both the acoustic attenuation and the potential influence of initial acoustic power density on the TFW.

First, let us consider Eqs. (4b) and (5b) in the lossless medium with $\alpha = 0$ and in the case of infinitely small signals, i.e., with $\sigma \to 0$. In so doing, one can estimate $G(x, \alpha = 0) = \eta x$, $G(0, \alpha = 0) = 0$, and write

$$|C_1(x)|^2 = \left(\frac{q_0(\sigma x)^2}{q_1}\right) \cdot \frac{\sin^2(\eta x)}{(\eta x)^2}, \tag{9}$$

where the distance x can be considered as a parameter. Historically, determination of the taken alone TFW for a collinear acousto-optical filter is connected with estimating its full width at half-maximum (FWHM); see, for instance, [2,3]. However, within resolving dense sets of neighboring lines in optical spectra, the widely used Rayleigh criterion could be preferable, and it will be exploited. The choice of a concrete criterion does not appear to be critically important, as one of them can be converted into the other one by the factor ~0.886 for the contour in Eq. (9). The Rayleigh criterion predicts in fact separating a pair of the neighboring $(\sin u/u)^2$-shaped distributions at the intensity level of $\nu \approx 0.405$. This is exactly the case of Eq. (9), and one has to resolve the transcendent algebraic equation $\sin(\eta x) = \nu^{1/2}(\eta x) \approx 0.6368(\eta x)$. The first (both positive and negative) solutions to this algebraic equation are $\eta_{(\pm)} x = \pm\pi/2$. They lead to the bandwidth from $\eta_{(-)} x = -\pi/2$ to $\eta_{(+)} x = +\pi/2$, i.e., to the full bandwidth at the intensity level $\nu \approx 0.405$, which is given by $\Delta\eta x = \eta_{(-)} x + \eta_{(+)} x = |-\pi/2| + |+\pi/2| = \pi$. Together with this a one-side mismatch, η had been previously [see Eqs. (1)] determined as $\eta = \Delta K/2 = \pi\delta f/V$, so that in more detailed form $\eta_{(\pm)} = \pi\delta f_{(\pm)}/V$ (where $\delta f_{(\pm)}$ are the corresponding one-side frequency deviations), and consequently, the total deviation of the mismatch is given by $\Delta\eta = \eta_{(-)} + \eta_{(+)} = \pi(\delta f_{(-)} + \delta f_{(+)})/V = \pi\delta f/V$. Combining the expressions, which include $\Delta\eta$, one arrives at the above-noted formula $\delta f = V/x$, where one can undoubtedly put $x = L$. Thus, one can see that the full width of the main lobe inherent in

the $(\sin u/u)^2$-distribution at the intensity level $\nu \approx 0.405$ gives the "standard" determination of the frequency resolution in acousto-optics or the TFW, which is conditioned by the limit $\sigma \to 0$. In the case of a moderately lossy medium, i.e., with $\alpha \neq 0$ and $\sigma \to 0$, Eqs. (2) give us

$$G(x, \alpha \neq 0) = \alpha^{-1}\eta[\alpha x - 1 + \ln(4\alpha\eta^{-1})], \tag{10a}$$

$$G(0, \alpha \neq 0) = \alpha^{-1}\eta[-1 + \ln(4\alpha\eta^{-1})]. \tag{10b}$$

As a result, $G(x, \alpha \neq 0) - G(0, \alpha \neq 0) = \eta x$ as well and one arrives at Eq. (9). Consequently, the traditional conclusion lies in the fact that under the condition of infinitely small signals, i.e., with $\sigma \to 0$, the acoustic losses do not affect the TFW independently on the concrete level of those linear losses.

Then, one can naturally consider Eq. (1b) in the case of $\alpha \neq 0$ under acting the signals of finite amplitude when $\sigma \neq 0$. The 3D plots peculiar to these distributions are presented in Fig. 5 for the scattered light intensity $|C_1(x)|^2$ in terms of absolute units in the practically reasonable approximation $q_0/q_1 \approx 1$ on the interval $0 \leq \sigma x \cong 3\pi$. Regular structures exhibit reaching a sequence of unit-valued maxima along the line $\eta x = 0$ within various dimensionless σx-periods depending on the product

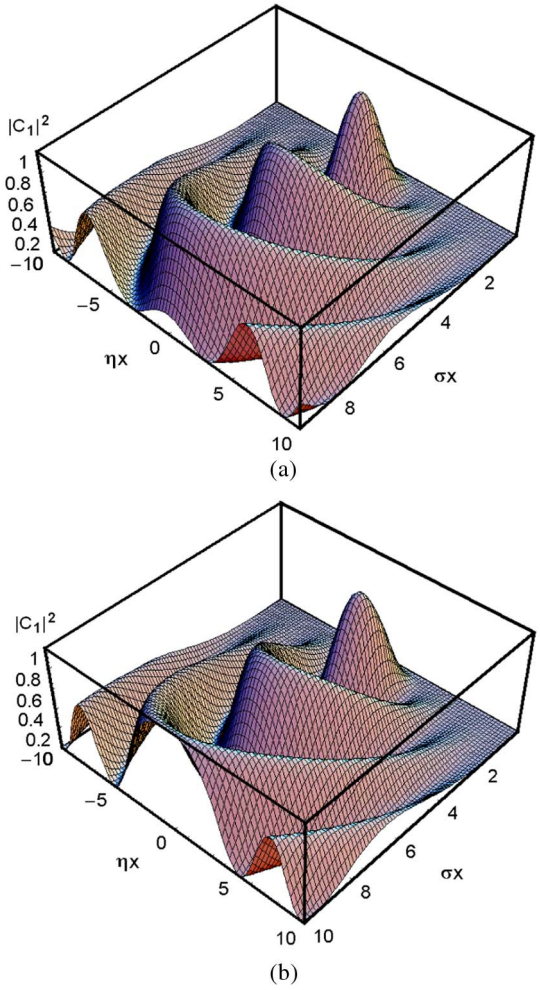

Fig. 5. 3D plots for the absolute values of the scattered light intensity profile with $\alpha \neq 0$ and $q_0/q_1 \approx 1$ on the interval $0 \leq \sigma x \cong 3\pi$: (a) $\alpha x = 0.1$ and (b) $\alpha x = 0.5$.

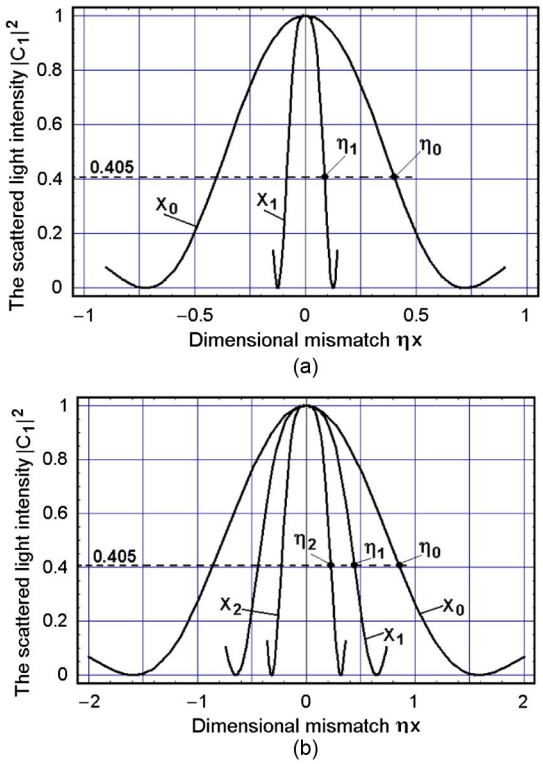

Fig. 6. 2D profiles $|C_1[(\sigma x), (\eta x)]|^2$ with $q_0/q_1 \approx 1$: (a) $\alpha = 0.1$ cm^{-1} and $\sigma = 0.5$ cm^{-1} with $X_0 = 3.768$ cm and $X_1 = 28.55$ cm, (b) $\alpha = 0.1$ cm^{-1} and $\sigma = 1$ cm^{-1} wherein $X_0 = 1.709$ cm, $X_1 = 6.372$ cm, and $X_2 = 15.39$ cm.

$\alpha x \neq 0$. In fact, one can consider the result of growing the product αx as a scaling along the σx axis, which leads to a shift of unit-valued maxima in the larger σx-direction.

Now, the TFW can be considered in a medium with moderate acoustical losses under the requirement of maximal efficiency. In the case of a moderate acoustical losses, Eqs. (1) and (2) should be exploited in their original forms as well with $\alpha \neq 0$ and $\sigma \neq 0$. The above-formulated requirement of maximal efficiency of light scattering leads to Eqs. (4) and (5) as well as to Figs. 1 and 2. Numerical simulations for 2D profiles of the intensities $|C_1(x)|^2$ with $q_0/q_1 \approx 1$ have been performed in three cases of moderate acoustical losses, namely (1) $\alpha = 0.1$ cm^{-1}, $\sigma = 0.5$ cm^{-1} (with $X_0 = 3.768$ cm and $X_1 = 28.55$ cm) and (2) $\alpha = 0.1$ cm^{-1}, $\sigma = 1$ cm^{-1} (with $X_0 = 1.709$ cm, $X_1 = 6.372$ cm, and $X_2 = 15.39$ cm); see 2D plots in Fig. 6. Thus the presence of moderate acoustical losses in a medium varies significantly the spatial scale of the light scattering processes. Together with this, a limited number of unit-valued maxima will appear as long as our approximate solution is valid. These circumstances make it necessary to estimate potential TFW in more detail.

4. COMBINED DIAGRAMS IN A MEDIUM WITH MODERATE ACOUSTICAL LOSSES

Finally, one can find that Eqs. (1) and (2) with $\alpha \neq 0$, $\sigma \neq 0$, and $q_0/q_1 \approx 1$ can be applied to create the first combined diagram. It can be obtained just for the totality of points with maximal scattered light intensity, which is theoretically equal to unity. In so doing, one can use Eq. (7) for determining the needed coordinates of maxima. Because each individual

maximum will be reached at $\eta = 0$, the contours of $|C_1(x)|^2$ need not additional normalization, so that one can consider the equation $|C_1(x)|^2 = 0.405$ for estimations to find a dependence of the expected one-side width η at the intensity level 0.405 on the applied acoustic power density σ with the loss parameter α. Introducing two ratios $R = \eta/\alpha$ and $S = \sigma/\alpha$ as new variables, one can rewrite that equation for estimations as

$$S^2 \cdot \sin^2\left(\sqrt{R^2+S^2} - \sqrt{R^2 + S^2\left[1 - \frac{\pi}{S}(N+0.5)\right]^2} - R\ln\left[1 - \frac{\pi}{S}(N+0.5)\right] + R\ln\left\{\frac{2}{R^2}\left[R + \sqrt{R^2 + S^2\left[1 - \frac{\pi}{S}(N+0.5)\right]^2}\right]\right\} - R\ln\left\{\frac{2}{R^2}\left[R + \sqrt{R^2+S^2}\right]\right\}\right) = 0.405 \cdot (R^2+S^2). \quad (11)$$

Results of numerical simulations for $N = 0, 1, 2, 3$ are presented in Fig. 7. This combined diagram can be easily interpreted with the fixed value of α resulting in a chosen material. With this in mind, the smaller the ratio $S = \sigma/\alpha$, needed for 100% efficiency of light scattering, the longer the length of acousto-optical interaction, which leads to narrower TFW, and vice versa. Then, with the fixed acoustical losses α, broadly speaking, exploiting higher orders N of light scattering promises improving the frequency resolution for an equivalent collinear acousto-optical filter (i.e., decreasing the ratio $R = \eta/\alpha$) when the ratio $S = \sigma/\alpha$ is fixed. However, such a conclusion becomes invalid for an area peculiar to minimal magnitudes of the ratio $S = \sigma/\alpha$, because one can see from Fig. 7 that for $S = \sigma/\alpha < 11$ not all the orders with numbers $N \le 3$ exist, and the last statement loses its meaning. Consequently, exploiting the lowest order $N = 0$ becomes the most profitable in a medium with moderate acoustical losses and from the viewpoint of minimizing the applied acoustic power density as well.

The second combined diagram appears through involving the other variables $s = \sigma x$, $r = \eta x$, and $a = \alpha x$ without supposing the requirement to reach just maxima. Now the above-noted equation for estimations has to be already normalized by $|C_1(\eta = 0)|^2$, so that one obtains

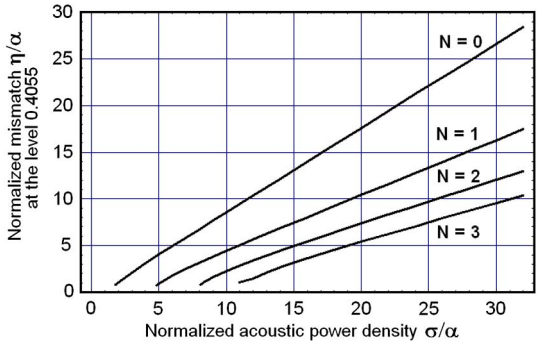

Fig. 7. First combined diagram expressed in the coordinates $R = \eta/\alpha$ and $S = \sigma/\alpha$ on a plane corresponding to the 0.405 level.

$$s^2 \cdot \sin^2\left(\frac{1}{a}\sqrt{r^2+s^2} - \frac{1}{a}\sqrt{r^2+s^2\exp[-a]} + \frac{r}{a}\ln\left\{\frac{2a}{r^2}\left[r\exp(a) + \sqrt{r^2\exp(2a)+s^2}\right]\right\} - \frac{r}{a}\ln\left\{\frac{2a}{r^2}\left[r + \sqrt{r^2+s^2}\right]\right\}\right) = 0.405 \cdot (r^2+s^2) \cdot \sin^2\left\{\frac{s}{a}[1-\exp(-a)]\right\}. \quad (12)$$

Results of numerical simulations of Eq. (12) for $a = \alpha x = 0.1$–2.0 are presented in Fig. 8. The parameter $r = \eta x$ corresponds to a half of the TFW, as discussed in Section 3 after Eq. (9). The scattered light intensity $|C_1(x)|^2$ is depicted here as well. One can see from Figs. 8 and 9 that the differences in the mismatches $r = \eta x$ belonging to various values of the parameter $a = \alpha x$ appear in contrast with the results of Section 3. This is why now one has to consider Eq. (12) in the case of infinitely small signal, i.e., with $\sigma \to 0$ or $s \to 0$. For this purpose, let us rewrite Eq. (12) as the equality of two ratios

$$\frac{1}{r^2+s^2} \cdot \sin^2\left(\frac{1}{a}\sqrt{r^2+s^2} - \frac{1}{a}\sqrt{r^2+s^2\exp[-a]} + \frac{r}{a}\ln\left\{\frac{2a}{r^2}\left[r\exp(a) + \sqrt{r^2\exp(2a)+s^2}\right]\right\} - \frac{r}{a}\ln\left\{\frac{2a}{r^2}\left[r + \sqrt{r^2+s^2}\right]\right\}\right) = 0.405 \cdot \frac{1}{s^2} \cdot \sin^2\left\{\frac{s}{a}[1-\exp(-a)]\right\}. \quad (13)$$

In the limit $s \to 0$, Eq. (13) gives

$$\frac{\sin^2(\eta x)}{(\eta x)^2} = 0.405 \cdot \left[\frac{1-\exp(-\alpha x)}{\alpha x}\right]^2. \quad (14)$$

One can see from Eq. (14) that, in contrast to the previously discussed traditional point of view, the TFW or the frequency resolution depends on acoustic losses even in the case of infinitely small controlling signal when $\sigma \to 0$ or $s \to 0$. Figure 10 shows the corresponding dimensionless dependence between the mismatch ηx and the acoustic losses αx for this case. With $\alpha x \to 0$, one arrives, of course, at the above-mentioned traditional estimation $\eta x \approx \pi/2$. One can find the correspondence

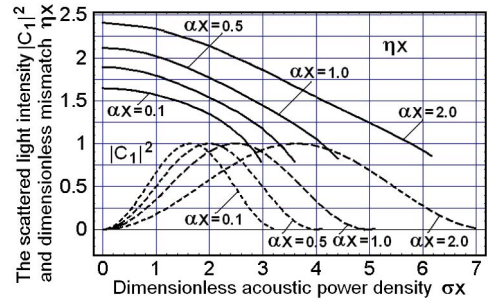

Fig. 8. Second combined diagram expressed in the coordinates $s = \sigma x$ and $r = \eta x$ with the parameter $a = \alpha x$ on a plane related to the 0.405 intensity level. The plots for the dimensionless mismatch ηx, which represents half of the TFW, are shown by solid lines. The plots for $|C_1(\eta = 0)|^2$ are drawn by dotted lines.

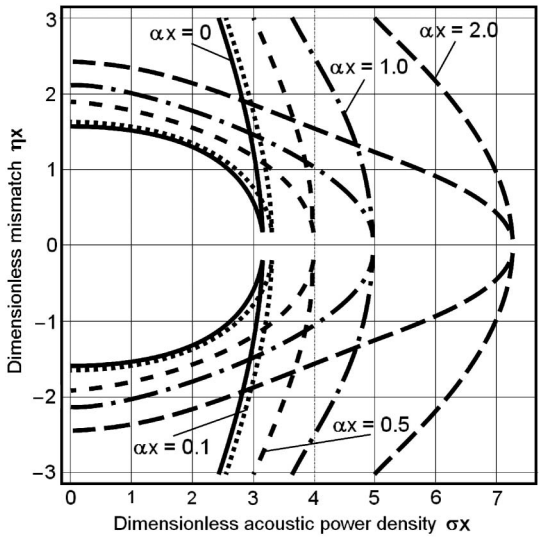

Fig. 9. Set of 2D plots for the normalized scattered light intensity $|C_1(x)|^2$ at the level of 0.405 on the plane $(\sigma x, \eta x)$ for various αx taken only within the first quasi-period.

between ηx–lines with $ox \to 0$ in Fig. 8 and the data from Fig. 10 at the same values of the acoustic losses αx. However, as long as the acoustic losses αx grow, one can observe an expansion of the normalized transfer function.

5. SOME ESTIMATIONS FOR THE CALCIUM MOLYBDATE OPTICAL CELL

Together with this, one can estimate the potential contributions of the acoustic losses. The coefficient of linear attenuation for the chosen pure shear acoustic mode, $\vec{K}\|[100]$, $\vec{u}\|[001]$, and $V = 2.95 \cdot 10^5$ cm/s, is $\Gamma = 60$ dB/(cm · GHz^2) in a calcium molybdate single crystal [16–18]. The factor α of the amplitude acoustic losses measured in cm^{-1} can be expressed via the relation $\alpha(\text{cm}^{-1}) = 0.1152 \cdot \Gamma(\text{dB/cm GHz}^2) \cdot f^2(\text{GHz})$. The carrier frequency f, peculiar to collinear acousto-optical interaction in calcium molybdate, depends on the light wavelength as $f = \Delta n \cdot V/\lambda$, where $\Delta n \approx 0.01$. At $\lambda_{\max} = 633$ nm, one can find $f_{\min} \approx 43.47$ MHz, so that one can estimate the amplitude factor of acoustic losses by $\gamma_{\min} = \Gamma(\text{dB/cm GHz}^2) \cdot f^2_{\min}(\text{GHz}) \approx 0.0844$ dB/cm, $\alpha_{\min} = 0.00972$ cm^{-1}, and $\alpha_{\min} L \approx 0.0428$. At $\lambda = 444$ nm, one can find $f_{\max} \approx 94.34$ MHz, so that

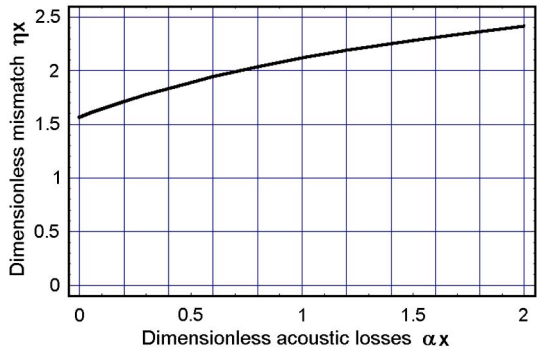

Fig. 10. Dimensionless mismatch ηx versus the acoustic losses αx with infinitely small controlling signal $\sigma \to 0$ or $s \to 0$.

one can estimate the acoustic losses by $\gamma_{\max} = \Gamma \cdot f^2_{\max} \approx 0.534$ dB/cm, $\alpha_{\max} = 0.1152 \cdot \gamma_{\max} \approx 0.06152$ cm^{-1}, and $\alpha_{\max} L \approx 0.271$. In the limit of $\sigma \to 0$, the aperture $L = 4.4$ cm leads to the TFW or to the frequency resolution $\delta f = V/L \approx 67.045$ kHz, at $f_{\max} \approx 94.34$ MHz, which gives the spectral resolution $\delta\lambda = V\lambda_{\min}/(f_{\max} L) \approx 3.1554 \cdot 10^{-8}$ cm ≈ 3.16 Å.

The maximal angular divergence of the acoustic beam in a calcium molybdate collinear cell will be undoubtedly observed at the lowest frequency $f = 43.47$ MHz. Practically, a reliable spatial size of the initial acoustic beam aperture that we will consider is close to $d \approx 0.2$ cm. Thus, one can find $\varphi = V/(fd) \approx 3.4 \cdot 10^{-2}$ rad $\approx 1.945°$ and conclude that the angular divergence of the acoustic beam can be definitely omitted. The full mismatch $\Delta\eta$ is connected with the TFW δf. Due to the above-mentioned expression $\Delta\eta = \pi\delta f/V$, one can find $\delta f = (\Delta\eta \cdot x)V/(\pi L)$. At this step, we are ready to perform a few practical numerical estimations inherent in collinear interaction at various light wavelengths of the visible range for the $CaMoO_4$-crystalline cell with the figure of acousto-optical merit $M_2 \approx 2 \cdot 10^{-18}$ (s^3/g).

Appearing both maxima and zeros in the light intensity, the $|C_1|^2$ distribution, described by Eq. (3), is characterized by Eqs. (5a) and (5b). They both can be obviously inverted as

$$\sigma_N^{(m)} = \frac{\alpha\pi(N + 0.5)}{1 - \exp(-\alpha X_N)}, \tag{15a}$$

$$\sigma_M^{(z)} = \frac{\alpha\pi M}{1 - \exp(-\alpha Z_M)}, \tag{15b}$$

so that, for example, with $\lambda = 532$ nm (green light), $f \approx 61.24$ MHz, and $\alpha \approx 0.026$ cm^{-1} one can find, at first, $\sigma_0^{(m)} \approx 0.38$ cm^{-1}, $\sigma_1^{(m)} \approx 1.13$ cm^{-1}, $\sigma_2^{(m)} \approx 1.90$ cm^{-1} > $\sigma_{\max} \approx 1.32$ cm^{-1} for $N = 0$, 1, 2 and $X_{1,2,3} = L = 4.4$ cm as well as then $\sigma_1^{(z)} \approx 0.7556$ cm^{-1} and $\sigma_2^{(z)} \approx 1.5112$ cm^{-1} > $\sigma_{\max} \approx 1.32$ cm^{-1} for $M = 1$, 2 and $Z_{1,2} = L = 4.4$ cm.

Using the determination introduced above, one can write

$$\sigma = U_0\sqrt{q_0 q_1} \approx \frac{\pi}{\lambda}\sqrt{\frac{P}{2}M_2}, \tag{16a}$$

$$P \approx \frac{2\lambda^2\sigma^2}{\pi^2 M_2}, \tag{16b}$$

where P is the acoustic power density. Equation (16b) gives $P[\text{W/mm}^2] \approx 0.287 \cdot (\sigma[\text{cm}^{-1}])^2$, so that maxima can be achieved with $P_0^{(m)} \approx 0.0410$ [W/mm^2] for $\sigma_0^{(m)}$, $P_1^{(m)} \approx 0.368$ [W/mm^2] for $\sigma_1^{(m)}$, and $P_2^{(m)} \approx 1.024$ [W/mm^2] > $P_{\max} = 0.5$ [W/mm^2] for $\sigma_2^{(m)}$, while zeros can be expected when $P_1^{(z)} \approx 0.164$ [W/mm^2] for $\sigma_1^{(z)}$ and $P_2^{(z)} \approx 0.655$ [W/mm^2] > $P_{\max} = 0.5$ [W/mm^2] for $\sigma_2^{(z)}$, respectively; see Fig. 11 and the theoretical plot in Fig. 13.

One can see that reaching the third maximum and the second zero requires too high acoustic power density in comparison with the previous extrema, so that it looks rather conjectural from the viewpoint of requirements to the electric strength inherent in the available piezoelectric transducer.

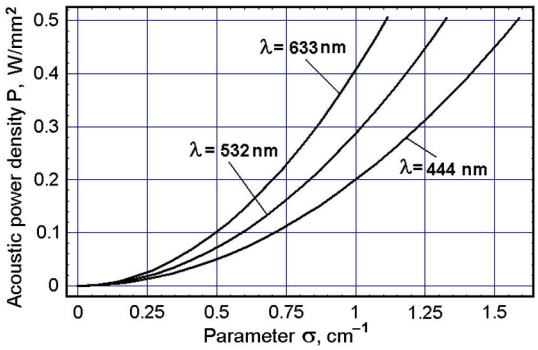

Fig. 11. Acoustic power density P versus the parameter σ in the $CaMoO_4$ cell.

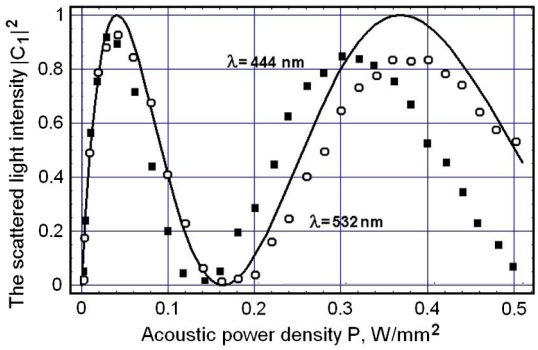

Fig. 13. Scattered light intensity $|C_1|^2$ versus the acoustic power density P with $\alpha = 0.0261$ cm^{-1} (solid line is for theory and circles are for experiment at $f = 61.24$ MHz, $\lambda = 532$ nm) and $\alpha = 0.0615$ cm^{-1} (squares are for experiment at $f_{\max} = 94.34$ MHz, $\lambda = 444$ nm) in the $CaMoO_4$-cell.

6. SCHEME FOR THE EXPERIMENTS WITH A CALCIUM MOLYBDATE CELL

To realize experimentally the process of collinear interaction, we have used the scheme shown in Fig. 12. It consists of a continuous-wave laser, a $CaMoO_4$-crystalline acousto-optical cell with a pair of Glan–Taylor crystalline polarizers (with the extinction ratio 10^5 each), a wide-aperture silicon photodetector, and a set of electronic equipment for both generating and registering the corresponding electric ultra-high-frequency (UHF) radio-wave signals. Initially, the tunable UHF signal is applied to the electronic input port of the collinear acousto-optical cell through a wide-band UHF amplifier HD18858 (10–1000 MHz, 8 W) (see Fig. 12), and to the input of an oscilloscope (computer) as the etalon signal.

A two-mode copropagating collinear $CaMoO_4$ crystalline cell was characterized by a crystal length $L = 4.4$ cm along the [100] axis, and acoustic velocity $V = 2.95 \cdot 10^5$ cm/s for the shear elastic mode whose displacement vector is oriented along the [001] axis. The continuous-wave beams (solid-state lasers from CrystaLaser; the output optical power ~30–40 mW; $\lambda = 444$, 532, and 633 nm; transverse mode TEMoo; single longitudinal mode, providing narrow enough optical spectral line) had been used as an optical pump during the experiments with the traveling-wave regime of interaction between the pumping light beam and the acoustic wave. It had been done, first, to keep just the visible range of operation with light beams simplifying the experimental conditions of observations. Then, the visible range of light overlaps a rather wide range of acoustic frequencies (35–95 MHz) and makes it accessible to vary the acoustic losses as much as possible (about five times) due to a square-law dependence of the attenuation on the frequency. Turning back to the scheme, the first polarizer was precisely aligned in correspondence with the optical axes of a crystal in a cell. As the optical pump

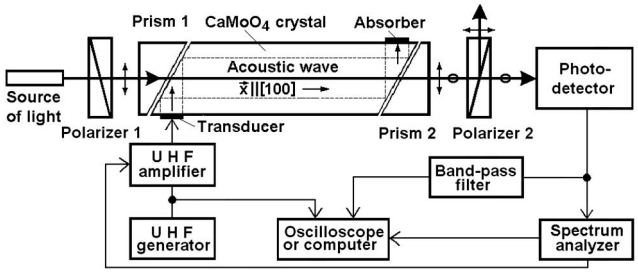

Fig. 12. Schematic arrangement of the experimental setup.

and the continuous-wave acoustic wave interacted, already two orthogonally polarized light beams, incident and signal ones, passed through a cell. The second polarizer gave us an opportunity to be aligned in correspondence with the polarization of the signal beam and to extract the output optical signal; see Fig. 12. Then, one can restrict oneself by a maximal level $P \le 0.5$ W/mm^2 of acoustic power density, which is conditioned by the absolute acoustic power magnitude of about 2 W and the acoustic beam cross section of about 4 mm^2 in the chosen collinear cell. Consequently, one can calculate that $\sigma \le 2$ cm^{-1}. These estimations demonstrate that the above-noted limitations on both the needed acoustic power densities and the magnitudes of the parameter σ, related to the firsts extrema, lie in the frames of acceptable values.

Not all the functional connections shown in Fig. 13 had been exploited at the same time. At least three regimes can be separated. One of them was related to measuring the light intensity dependences at the fixed acoustic carrier frequency. Two others were connected by estimating the frequency dependencies at stepwise variations of the applied acoustic power. They both include exploitation of the sweep generator from the spectrum analyzer and provide operation with the band-pass filter (bandwidth ~5 kHz) and oscilloscope as well as with the spectrum analyzer (bandwidth ≤10 Hz), in particular for calibrations and accurate measurements of frequency.

7. DISCUSSION AND CONCLUDING REMARKS

The nonlinear dynamics of varying the transmission functions peculiar to the advanced collinear $CaMoO_4$ acousto-optical cell have been sequentially followed during our experiments. A triplet of experiments had been carried out. First, the scattered light intensity $|C_1|^2$ as a function of the acoustic power density P with a fixed length of interaction $L = 4.4$ cm was registered under the condition of $P \le 0.5$ W/mm^2 (i.e., $\sigma \le 2$ cm^{-1}). To identify better the expected influence of moderate linear losses on the transmission functions of that cell, the maximal acceptable acoustic frequency $f_{\max} = 94.34$ MHz, accompanied by $\lambda = 444$ nm, was chosen to provide the highest possible acoustic attenuation for this cell, $\alpha = 0.1152 \cdot \Gamma f_{\max}^2 \approx 0.0615$ cm^{-1}. For comparison, the similar plot for $\alpha = 0.0261$ cm^{-1} related to $f = 61.24$ MHz and $\lambda = 532$ nm has been chosen. The corresponding

experimental plots are depicted in Fig. 13. One can see that a few extrema, namely two maxima and one zero, were achieved at each optical wavelength and were registered while the measurements were being carried out. The here-presented trace for $\lambda = 532$ nm can be compared with the theoretical plot.

Merely the presence of moderate linear acoustic losses is able to affect the width of the transmission function. Reshaping the transmission function has been followed with approximately the same input optical pumps at various light wavelengths and at almost the same values of the product σL, which all can be characterized as "rather small" in a view of realizing a limit to infinitely small input acoustic signals. To keep a balance between the lowest acceptable levels of acoustic power in that limit, on the one hand, and to have an option for reliable measurements of the TFW, on the other hand, the product $\sigma L \approx 0.2$ was chosen experimentally. In fact, fixing this product leads, nevertheless, to $\sigma = 0.04545$ cm^{-1} and remarkably different levels of the needed acoustic power densities $P[\mathrm{W/cm^2}] \approx 0.27 \cdot (\lambda[\mu\mathrm{m}])^2$ for its realization. Using Eq. (16b) for $\lambda_{A,B,C} = \{633, 532, 444(\mathrm{nm})\}$ connected with $f_{A,B,C} = \{43.47, 61.24, 94.34(\mathrm{MHz})\}$, one can find $P_{A,B,C} = \{1.082, 0.764, 0.533(\mathrm{mW/mm^2})\}$ and the products $(\alpha L)_{A,B,C} \approx \{0.0575, 0.114, 0.271\}$, respectively. Then, exploiting Eq. (14) and Fig. 10, one can estimate theoretically the mismatches ηx as a function of the total acoustic losses αL at various frequencies as $(\eta x)_A = 1.614$, $(\eta x)_B = 1.656$, and $(\eta x)_A = 1.761$, which give theoretically $\delta f_A = 68.89$ kHz, $\delta f_B = 70.53$ kHz, and $\delta f_C = 75.15$ kHz.

A few examples of the corresponding digitized oscilloscope traces, estimated at the level of 0.405 conditioned by the Rayleigh criterion, are shown in Fig. 14. These traces for

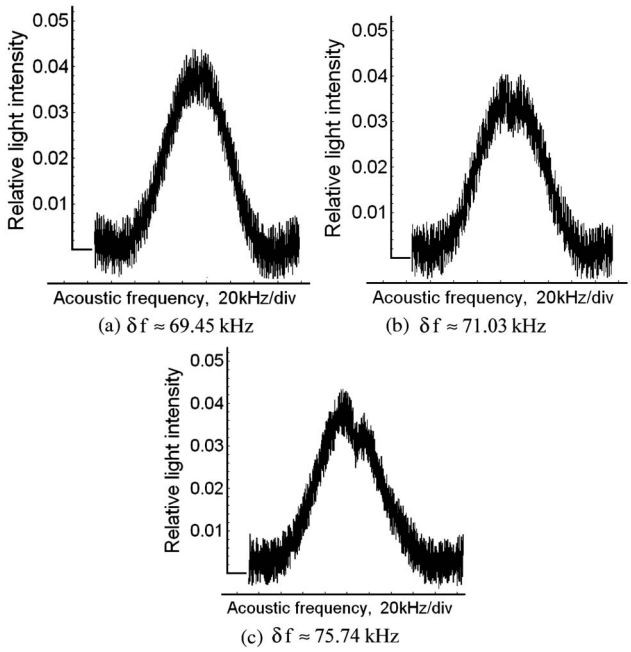

Fig. 14. Digitized oscilloscope traces for the scattered light intensity $|C_1|^2$ observed at the output of the collinear $CaMoO_4$ cell for various acoustic losses and acoustic frequencies. Their widths have been measured at the level 0.405 with $\sigma L \approx 0.2$, so that (a) $f_A = 43.47$ MHz, $(\alpha L)_A \approx 0.0575$; (b) $f_B = 61.24$ MHz, $(\alpha L)_B \approx 0.114$; and (c) $f_C = 94.34$ MHz, $(\alpha L)_C \approx 0.271$.

the scattered light intensity $|C_1|^2$ had been observed at the output of the above-described collinear $CaMoO_4$ cell at various carrier acoustic frequencies, which provide various magnitudes of the linear acoustic losses depending quadratically on those frequencies.

Finally, the effect of nonlinear narrowing was observed via measuring the widths peculiar to profiles of the scattered light intensity $|C_1|^2$ as a function of the applied acoustic power density explained in terms of the dimensionless product σL. For this purpose, we had taken the regime of scattering the green light with $\lambda = 532$ nm connected with the acoustic wave frequency $f_0 = 61.24$ MHz, which provides sufficiently tangible total acoustic attenuation $\alpha L \approx 0.114$ all over the cell aperture. First, both of the 2D-theoretical plots with the product $\alpha L \approx \{0, 0.0575, 0.114, 0.271\}$ and the observed experimental data as points are combined in Fig. 15.

Then, we observed the oscilloscope traces for the scattered light component intensity $|C_1|^2$ detected during the experiments with the collinear $CaMoO_4$ crystalline cell and estimated at the level 0.405 conditioned by the Rayleigh criterion; see Fig 16. All these traces can be interpreted in terms of the above-developed theory.

The leftmost left triplet of experimental points in Fig. 15 corresponds to $\sigma L \approx 0.20$, which is very close to zero. They reflect the transmission functions inherent in the regime with almost infinitely small amplitude of the controlling acoustic signal. This value σL (which is nonzero, in fact) had been taken as an example to show an adequately conventional representation for the TFW being reasonably close to the traditional estimation $\delta f \approx V/L = 67.045$ kHz in our case, as well as to have a chance for identifying the output light distributions whose relative intensities were small enough, i.e., about 3.5%. This triplet of points had been discussed above and illustrated by the corresponding oscilloscope traces in Fig. 14 related to the three different light wavelengths. All the other points in Fig. 15 are related to only $\lambda = 532$ nm with varying product σL.

The points peculiar to $\sigma L \approx \{0.5, 1.0, \pi/2\}$ are presented in Fig. 15, and the last of them is illustrated by the oscilloscope

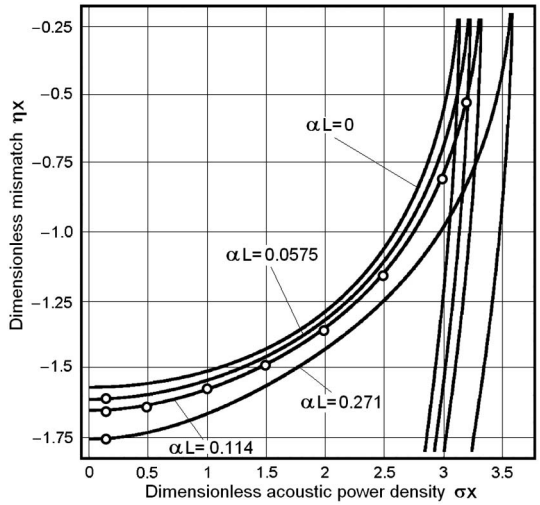

Fig. 15. Combined diagram reflecting both the 2D-theoretical plots with the product $\alpha L \approx \{0, 0.0575, 0.114, 0.271\}$ and all the above-noted experimental points. The lossless case is $\alpha L = 0$.

trace in Fig. 16(a). From the viewpoint of the widely used acousto-optic approach, they can be considered as a natural testimony of growing the relative intensity of the output optical signal up to the products σL equal to 0.202, 0.657, and ~1.0 under action of the increasing acoustic power density. They all exhibit a TFW of more or less the same order, which varies slightly from the above-mentioned 71.03 kHz to $\delta f \approx 70.42$ kHz, $\delta f \approx 67.84$ kHz, and $\delta f \approx 64.04$ kHz for $\sigma L \approx \{0.5, 1.0, \pi/2\}$, respectively.

The numerical estimations are given by the values $\delta f = 69.81$ kHz, $\delta f = 67.34$ kHz, and $\delta f = 63.40$ kHz at the same σL. Such a conclusion looks rather plausible within quasi-linear approximation for the transmission function as well as in the course of possible measurements in the frequency domain with not enough accuracy. Nevertheless, further increase of the acoustic power density, depicted by the points with $\sigma L \approx 2.0$ and $\sigma L \approx 2.5$ in Fig. 15 and the oscilloscope trace in Fig. 16(b), is able to demonstrate step by step that the existing specific acousto-optical nonlinearity leads to narrowing the transmission function to $\delta f \approx 58.46$ kHz and $\delta f \approx 50.17$ kHz, respectively, while theoretically one can find $\delta f \approx 57.67$ kHz and $\delta f \approx 48.987$ kHz. This process is accompanied by decreasing the relative intensity of the output optical beam down to about 0.9 and 0.5 in the so-chosen points. Finally, the last traces [see Fig. 15 as well as Figs. 16(c) and 16(d)] illustrate obviously the nonlinear process of narrowing the transmission function or improving the frequency resolution in the vicinity of the first point $\sigma L = \pi$ of a collapse. Namely the values $\sigma L \approx 3.0$ and $\sigma L \approx 3.20$ have been taken to have an opportunity for revealing the transmission function characterized by $\delta f \approx 34.13$ kHz and even $\delta f \approx 21.95$ kHz (theoretically $\delta f \approx 33.46$ kHz and $\delta f \approx 21.52$ kHz) whose relative intensities have already become very small and do not exceed 0.09 and 0.01, respectively.

Thus, one can conclude that we have revealed nonlinear narrowing of the transmission function inherent in collinear acousto-optical interaction occurred by the acoustic waves in a medium with moderate losses. This nonlinear effect can also be interpreted as improving the spectral and frequency resolution peculiar to the equivalent collinear acousto-optical filter operated by the controlling acoustic waves of finite amplitude. In fact, we have found an opportunity to exchange a portion of transmittance for a portion of accuracy. Sometimes, for instance in astrophysical observations, it could be useful practically when an extremely bright object is under optical spectrum analysis. Rather adequate theory of this effect has been developed analytically and illustrated via the corresponding computer simulations. In particular, a periodicity for the nonlinear narrowing of the transmission function, which includes a set of points for its collapses originating periodically, has been found and estimated. It has been shown that the first period of similar collapsing exhibits the best relation between the width and magnitude of the narrowed transmission function from the viewpoint of practical application. Then, the needed estimations have been performed for collinear interaction in the visible range in a $CaMoO_4$ crystal. The results of our experiments illustrating the nonlinear narrowing of the transmission function within propagation of acoustic waves with moderate losses in the collinear calcium molybdate crystalline cell have been presented and briefly discussed.

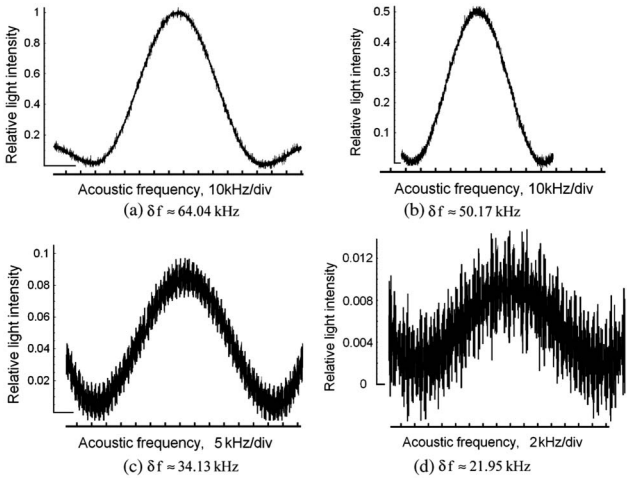

Fig. 16. Digitized oscilloscope traces for the scattered light intensity $|C_1|^2$ for the green light with $\lambda = 532$ nm observed at the output of the collinear $CaMoO_4$ cell near the central carrier acoustic frequency $f_0 = 61.24$ MHz and estimated at the level 0.405. Reshaping the transmission function is followed at the same optical pump in variable scales: (a) $\sigma L \approx \pi/2$, $P \approx 0.0365$ [W/mm^2]; (b) $\sigma L \approx 2.5$, $P \approx 0.0925$ [W/mm^2]; (c) $\sigma L \approx 3.0$, $P \approx 0.133$ [W/mm^2]; and (d) $\sigma L \approx 3.2$, $P \approx 0.152$ [W/mm^2].

ACKNOWLEDGMENTS

This work was supported by CONACyT (project no. 61237).

REFERENCES

1. R. W. Dixon, "Acoustic diffraction of light in anisotropic media," IEEE J. Quantum Electron. **QE-3**, 85–93 (1967).
2. S. E. Harris and R. W. Wallace, "Acousto-optic tunable filter," J. Opt. Soc. Am. **59**, 744–747 (1969).
3. S. E. Harris, S. T. K. Nich, and R. S. Fiegelson, "$CaMoO_4$ electronically tunable optical filter," Appl. Phys. Lett. **17**, 223–225 (1970).
4. I. C. Chang, "Tunable acousto-optic filter utilizing acoustic beam walk-off in crystal quartz," Appl. Phys. Lett. **25**, 323–324 (1974).
5. J. A. Kusters, D. A. Wilson, and D. L. Hammond, "Optimum crystal orientation for acoustically tuned optical filters," J. Opt. Soc. Am. **64**, 434–440 (1974).
6. E. T. Aksenov, N. A. Esepkina, and A. S. Shcherbakov, "Acousto-optical filter with a $LiNbO_3$-crystal," Tech. Phys. Lett. **2**, 83–84 (1976).
7. J. D. Fichter, M. Gottlieb, and J. J. Conroy, "Tl_3AsSe_3 noncollinear acousto-optic filter operation at 10 μm," Appl. Phys. Lett. **34**, 1–3 (1979).
8. V. N. Parygin, A. V. Vershubskii, and K. A. Kholostov, "Control of the characteristics of a calcium molybdate collinear acousto-optic filter," Tech. Phys. **44**, 1467–1471 (1999).
9. V. I. Balakshy, V. N. Parygin, and L. I. Chrkov, *Physical Principles of Acousto-Optics* (Radio I Svyaz, 1985).
10. A. Korpel, *Acousto-Optics*, 2nd ed. (Dekker, 1997).
11. F. T. S. Yu, *Introduction to Information Optics* (Academic, 2001).
12. See, for example A. Mahieux, V. Wilquet, R. Drummond, D. Belyaev, A. Federova, and A. C. Vandaele, "A new method for determining the transfer function of an acousto optical tunable filter," Opt. Express **17**, 2005–2014 (2009).
13. A. S. Shcherbakov and A. Aguirre Lopez, "Shaping the optical components of solitary three-wave weakly coupled states in a two-mode waveguide," Opt. Express **11**, 1643–1649 (2003).
14. A. S. Shcherbakov and A. Aguirre Lopez, "Binary encoded modulation of light based on collinear three-wave

acousto-optical weakly coupled states," J. Opt. A **5**, 471–477 (2003).
15. A. S. Shcherbakov, J. Maximov, and S. E. Balderas Mata, "Shaping the dissipative collinear three-wave coupled states in a two-mode medium with a square-law nonlinearity and linear non-optical losses," J. Opt. A **10**, 025001 (2008).
16. M. P. Shaskolskaya, ed., *Handbook "Acoustic Crystals"* (Nauka, 1988).
17. V. G. Dmitriev, G. G. Gurzadyan, and D. N. Nikogosyan, *Handbook of Nonlinear Optical Crystals* 3rd ed. (Springer, 1999).
18. A. A. Blistanov, *Crystals for Quantum and Nonlinear Optics*, 2nd ed. (MISIS, 2007).